Anticancer immunotherapy by CTLA-4 blockade relies on the gut microbiota

Marie Vétizou, Jonathan M. Pitt, Romain Daillere, Patricia Lepage, Nadine Waldschmitt, Caroline Flament, Sylvie Rusakiewicz, Bertrand Routy, Maria P. Roberti, Connie P. M. Duong, et al.

HHS Public Access

Author manuscript

Science. Author manuscript; available in PMC 2016 January 21.

Published in final edited form as:

Science. 2015 November 27; 350(6264): 1079–1084. doi:10.1126/science.aad1329.

Anticancer immunotherapy by CTLA-4 blockade relies on the gut microbiota

Marie Vétizou[1,2,3], **Jonathan M. Pitt**[1,2,3], **Romain Daillère**[1,2,3], **Patricia Lepage**[4], **Nadine Waldschmitt**[5], **Caroline Flament**[1,2,6], **Sylvie Rusakiewicz**[1,2,6], **Bertrand Routy**[1,2,3,6], **Maria P. Roberti**[1,2,6], **Connie P. M. Duong**[1,2,6], **Vichnou Poirier-Colame**[1,2,6], **Antoine Roux**[1,2,7], **Sonia Becharef**[1,2,6], **Silvia Formenti**[8], **Encouse Golden**[8], **Sascha Cording**[9], **Gerard Eberl**[9], **Andreas Schlitzer**[10], **Florent Ginhoux**[10], **Sridhar Mani**[11], **Takahiro Yamazaki**[1,2,6], **Nicolas Jacquelot**[1,2,3], **David P. Enot**[1,7,12], **Marion Bérard**[13], **Jérôme Nigou**[14,15], **Paule Opolon**[1], **Alexander Eggermont**[1,2,16], **Paul-Louis Woerther**[17], **Elisabeth Chachaty**[17], **Nathalie Chaput**[1,18], **Caroline Robert**[1,16,19], **Christina Mateus**[1,16], **Guido Kroemer**[7,12,20,21,22], **Didier Raoult**[23], **Ivo Gomperts Boneca**[24,25,*], **Franck Carbonnel**[3,26,*], **Mathias Chamaillard**[5,*], and **Laurence Zitvogel**[1,2,3,6,†]

[1]Institut de Cancérologie Gustave Roussy Cancer Campus (GRCC), 114 rue Edouard Vaillant, 94805 Villejuif, France

[2]INSERM U1015, GRCC, Villejuif, France

[3]University of Paris Sud XI, Kremlin-Bicêtre, France

[4]Institut National de la Recherche Agronomique (INRA), Micalis-UMR1319, 78360 Jouy-en-Josas, France

[5]University of Lille, CNRS, INSERM, Centre Hospitalier Régional Universitaire de Lille, Institut Pasteur de Lille, U1019, UMR 8204, Centre d'Infection et d'Immunité de Lille (CIIL), F-59000 Lille, France

[6]Center of Clinical Investigations in Biotherapies of Cancer 1428, Villejuif, France

[7]Université Paris Descartes, Sorbonne Paris Cité, Paris, France

[8]Department of Radiation Oncology, New York University, New York, NY, USA

[9]Microenvironment and Immunity Unit, Institut Pasteur, Paris, France

[10]Singapore Immunology Network (SIgN), Agency for Science, Technology and Research (A*STAR), Singapore, Singapore

[11]Department of Genetics and Department of Medicine, Albert Einstein College of Medicine, Bronx, NY 10461, USA

[†]Corresponding author. laurence.zitvogel@gustaveroussy.fr.

[*]These authors contributed equally to this work.

SUPPLEMENTARY MATERIALS

www.sciencemag.org/content/350/6264/1079/suppl/DC1 Materials and Methods

Figs. S1 to S22

Tables S1 to S5

References (19–35)

[12]Metabolomics Platform, GRCC, Villejuif, France

[13]Animalerie Centrale, Institut Pasteur, Paris, France

[14]Centre National de la Recherche Scientifique, Institut de Pharmacologie et de Biologie Structurale (IPBS), Toulouse, France

[15]Université de Toulouse, Université Paul Sabatier, IPBS, F-31077 Toulouse, France

[16]Department of Medical Oncology, Institut Gustave Roussy, Villejuif, France

[17]Service de microbiologie, GRCC, Villejuif, France

[18]Laboratory of Immunomonitoring in Oncology, UMS 3655 CNRS/US 23 INSERM, GRCC, Villejuif, France

[19]INSERM U981, GRCC, Villejuif, France

[20]INSERM U848, Villejuif, France

[21]Equipe 11 Labellisée—Ligue Nationale contre le Cancer, Centre de Recherche des Cordeliers, INSERM U1138, Paris, France

[22]Pôle de Biologie, Hôpital Européen Georges Pompidou, Assistance Publique—Hôpitaux de Paris, Paris, France

[23]Unité des Rickettsies, Faculté de Médecine, Université de la Méditerranée, Marseille, France

[24]Institut Pasteur, Unit of Biology and Genetics of the Bacterial Cell Wall, Paris, France

[25]INSERM, Equipe Avenir, Paris, France

[26]Gastroenterology Department, Hôpital Bicêtre, Assistance Publique—Hôpitaux de Paris, Paris, France

Abstract

Antibodies targeting CTLA-4 have been successfully used as cancer immunotherapy. We find that the antitumor effects of CTLA-4 blockade depend on distinct *Bacteroides* species. In mice and patients, T cell responses specific for *B. thetaiotaomicron* or *B. fragilis* were associated with the efficacy of CTLA-4 blockade. Tumors in antibiotic-treated or germ-free mice did not respond to CTLA blockade. This defect was overcome by gavage with *B. fragilis*, by immunization with *B. fragilis* polysaccharides, or by adoptive transfer of *B. fragilis*–specific T cells. Fecal microbial transplantation from humans to mice confirmed that treatment of melanoma patients with antibodies against CTLA-4 favored the outgrowth of *B. fragilis* with anticancer properties. This study reveals a key role for *Bacteroidales* in the immunostimulatory effects of CTLA-4 blockade.

Ipilimumab is a fully human monoclonal antibody (Ab) directed against CTLA-4, a major negative regulator of T cell activation (1), approved in 2011 for improving the overall survival of patients with metastatic melanoma (MM) (2). However, blockade of CTLA-4 by ipili-mumab often results in immune-related adverse events at sites that are exposed to commensal microorganisms, mostly the gut (3). Patients treated with ipilimumab develop Abs to components of the enteric flora (4). Therefore, given our previous findings for other

cancer therapies (5), addressing the role of gut microbiota in the immunomodulatory effects of CTLA-4 blockade is crucial for the future development of immune checkpoint blockers in oncology.

We compared the relative therapeutic efficacy of the CTLA-4–specific 9D9 Ab against established MCA205 sarcomas in mice housed in specific pathogen–free (SPF) versus germ-free (GF) conditions. Tumor progression was controlled by Ab against CTLA-4 in SPF but not in GF mice (Fig. 1, A and B). Moreover, a combination of broad-spectrum antibiotics [ampicillin + colistin + streptomycin (ACS)] (Fig. 1C), as well as imipenem alone (but not colistin) (Fig. 1C), compromised the antitumor effects of CTLA-4–specific Ab. These results, which suggest that the gut microbiota is required for the anticancer effects of CTLA-4 blockade, were confirmed in the Ret melanoma and the MC38 colon cancer models (fig. S1, A and B). In addition, in GF or ACS-treated mice, activation of splenic effector $CD4^+$ T cells and tumor-infiltrating lymphocytes (TILs) induced by Ab against CTLA-4 was significantly decreased (Fig. 1, D and E, and fig. S1, C to E).

We next addressed the impact of the gut micro-biota on the incidence and severity of intestinal lesions induced by CTLA-4 Ab treatment. A “subclinical colitis” dependent on the gut microbiota was observed at late time points (figs. S2 to S5). However, shortly (by 24 hours) after the first administration of CTLA-4 Ab, we observed increased cell death and proliferation of intestinal epithelial cells (IECs) residing in the ileum and colon, as shown by immunohistochemistry using Ab-cleaved caspase-3 and Ki67 Ab, respectively (Fig. 2A and fig. S6A). The CTLA-4 Ab–induced IEC proliferation was absent in RegIIIβ-deficient mice (fig. S6A). Concomitantly, the transcription levels of *Il17a*, *Ifng*, *Ido1*, *type 1 Ifn*-related gene products and *Ctla4* (but not *Il6*), which indicate ongoing inflammatory processes, significantly increased by 24 hours in the distal ileum of CTLA-4 Ab–treated mice (fig. S6, B to D). Depletion of T cells, including intraepithelial lymphocytes (IELs) (by injection of Abs specific for CD4 and CD8), abolished the induction of IEC apoptosis by CTLA-4–specific Ab (Fig. 2A). When crypt-derived three-dimensional small intestinal enteroids (6) were exposed to Toll-like receptor (TLR) agonists (which act as microbial ligands in this assay) and subsequently admixed with IELs harvested from mice treated with Ab against CTLA-4 (but not isotype Ctl), IECs within the enteroids underwent apoptosis (Fig. 2B). Hence, CTLA-4 Ab compromises the homeostatic IEC-IEL equilibrium, favoring the apoptotic demise of IEC in the presence of microbial products.

To explore whether this T cell–dependent IEC death could induce perturbations of the microbiota composition, we performed high-throughput pyrosequencing of 16*S* ribosomal RNA (rRNA) gene amplicons of feces. The principal component analysis indicated that a single injection of CTLA-4 Ab sufficed to significantly affect the microbiome at the genus level (Fig. 2C). CTLA-4 blockade induced a rapid underrepresentation of both *Bacteroidales* and *Burkholderiales*, with a relative increase of *Clostridiales*, infeces (Fig. 2C and table S1). Quantitative polymerase chain reaction (QPCR) analyses targeting the *Bacteroides* genus and species (spp.) in small intestine mucosa and feces contents showed a trend toward a decreased relative abundance of such bacteria in the feces, which contrasted with a relative enrichment in particular species [such as *B. thetaiotaomicron* (*Bt*) and *B. uniformis*] in the small intestine mucosa 24 to 48 hours after one CTLA-4 Ab injection (Fig. 2D and fig. S7).

One of the most regulatory *Bacteroides* isolates, *B. fragilis* (*Bf*) (7–10), was detectable by PCR in colon mucosae but was not significantly increased with CTLA-4 Ab (fig. S7).

Next, to establish a cause-and-effect relationship between the dominance of distinct *Bacteroides* spp. in the small intestine and the anticancer efficacy of CTLA-4 blockade, we recolonized ACS-treated and GF mice with several bacterial species associated with CTLA-4 Ab–treated intestinal mucosae as well as *Bf*. ACS-treated mice orally fed with *Bt*, *Bf*, *Burkholderia cepacia* (*Bc*), or the combination of *Bf* and *Bc*, recovered the anticancer response to CTLA-4 Ab, contrasting with all the other isolates that failed to do so (table S2 and Fig. 3A). Similarly, oral feeding with *Bf*, which colonized the mucosal layer of GF mice (fig. S8) (11), induced T helper 1 (TH_1) immune responses in the tumor-draining lymph nodes and promoted the maturation of intratumoral dendritic cells (DCs), which culminated in the restoration of the therapeutic response of GF tumor bearers to CTLA-4 Ab (Fig. 3B and fig. S9, A and B).

We analyzed the dynamics of memory T cell responses directed against distinct bacterial species in mice and humans during CTLA-4 blockade. $CD4^+$ T cells harvested from spleens of CTLA-4 Ab–treated mice (Fig. 3C) or from blood taken from individuals with MM or non–small cell lung carcinoma (NSCLC) patients after two administrations of ipilimumab (Fig. 3, D and E, and table S3) tended to recover a TH_1 phenotype (figs. S10 and S11). The functional relevance of such T cell responses for the anticancer activity of CTLA-4 Ab was further demonstrated by the adoptive transfer of memory *Bf*-specific (but not *B. distasonis*-specific) TH_1 cells into GF or ACS-treated tumor bearers (Fig. 3F and fig. S12), which partially restored the efficacy of the immune checkpoint blocker.

The microbiota-dependent immunostimulatory effects induced by CTLA-4 blockade depended on the mobilization of lamina propria $CD11b^+$ DC that can process zwitterionic poly-saccharides (9) and then mount interleukin-12 (IL-12)–dependent cognate TH_1 immune responses against *Bf* capsular polysaccharides (figs. S13 and S14). However, they did not appear to result from TLR2/TLR4-mediated innate signaling (7, 8) in the context of a compromised gut tolerance (figs. S15 to S19).

To address the clinical relevance of these findings, we analyzed the composition of the gut microbiome before and after treatment with ipilimumab in 25 individuals with MM (table S4). A clustering algorithm based on genus composition of the stools (12, 13) distinguished three clusters (Fig. 4A and table S5) with *Al-loprevotella or Prevotella* driving cluster A and distinct *Bacteroides* spp. driving clusters B and C (Fig. 4B). During ipilimumab therapy, the proportions of MM patients falling into cluster C increased, at the expense of those belonging to cluster B (Fig. 4B and fig. S20A). We next performed fecal microbial transplantation of feces harvested from different MM patients from each cluster, 2 weeks before tumor inoculation into GF mice that were subsequently treated with anti–CTLA-4 Ab. Tumors growing in mice that had been transplanted with feces from cluster C patients markedly responded to CTLA-4 blockade, contrasting with absent anticancer effects in mice transplanted with cluster B–related feces (Fig. 4C). QPCR analyses revealed that, although bacteria from the *Bacteroidales* order equally colonized the recipient murine intestine, stools from cluster C (but not A or B) individuals specifically facilitated the colonization of the

immunogenic bacteria *Bf* and *Bt* (7–10, 14, 15) (Fig. 4D). Moreover, after CTLA-4 Ab therapy, only cluster C (not A or B) recipient mice had outgrowth of *Bf* (fig. S20B). Note that the fecal abundance of *Bf* (but not *B. distasonis* or *B. uniformis*) negatively correlated with tumor size after CTLA-4 blockade in cluster C–recipient mice (Fig. 4E and fig. S20C). Hence, ipilimumab can modify the abundance of immunogenic *Bacteroides* spp. in the gut, which in turn affects its anticancer efficacy.

Finally, intestinal reconstitution of ACS-treated animals with the combination of *Bf* and *Bc* did not increase but rather reduced histopathological signs of colitis induced by CTLA-4 blockade (Fig. 3A). This efficacy-toxicity uncoupling effect was not achieved with vancomycin, which could boost the antitumor effects of CTLA-4 blockade (presumably by inducing the overrepresentation of *Bacteroidales* at the expense of *Clostridiales*) but worsened the histopathological score (fig. S21). In support of this notion, *Bf* maintained its regulatory properties in the context of CTLA-4 blockade (fig. S22) (7).

Hence, the efficacy of CTLA-4 blockade is influenced by the microbiota composition (*B. fragilis* and/or *B. thetaiotaomicron* and *Burkholderiales*). The microbiota composition affects interleukin 12 (IL-12)–dependent TH_1 immune responses, which facilitate tumor control in mice and patients while sparing intestinal integrity. In accord with previous findings (16), colitis (observed in the context of IL-10 deficiency and CTLA-4 blockade) (fig. S17) could even antagonize anti-cancer efficacy. Several factors may dictate why such commensals could be suitable “anticancer probiotics.” The geodistribution of *Bf* in the mucosal layer of the intestine (fig. S8) and its association with *Burkholderiales*—recognized through the pyrin–caspase-1 inflammasome (17) and synergizing with TLR2/TLR4 signaling pathways (fig. S15) —may account for the immunomodulatory effects of CTLA-4 Ab. Future investigations will determine whether a potential molecular mimicry between distinct commensals and/or pathobionts and tumor neoantigens could account for the toxicity and/or efficacy of immune checkpoint blockers. Prospective studies in MM and/or NSCLC may validate the relevance of the enterotypes described herein in the long-term efficacy of immune checkpoint blockers, with the aim of compensating cluster B–driven patients with live and immunogenic or recombinant *Bacteroides* spp. (18) or fecal microbial transplantation from cluster C–associated stools to improve their antitumor immune responses.

Supplementary Material

Refer to Web version on PubMed Central for supplementary material.

Acknowledgments

We are grateful to the staff of the animal facility of Gustave Roussy and Institut Pasteur. The data presented in this manuscript are tabulated in the main paper and in the supplementary materials. L.Z., M.V., and P.L. have filed patent application no. EP 14190167 that relates to the following: Methods and products for modulating microbiota composition for improving the efficacy of a cancer treatment with an immune checkpoint blocker. M.V. and J.M.P. were supported by La Ligue contre le cancer and ARC, respectively. L.Z. received a special prize from the Swiss Bridge Foundation and ISREC. G.K. and L.Z. were supported by the Ligue Nationale contre le Cancer (Equipes labelisées), Agence Nationale pour la Recherche (ANR AUTOPH, ANR Emergence), European Commission (ArtForce), European Research Council Advanced Investigator Grant (to G.K.), Fondation pour la Recherche Médicale (FRM), Institut National du Cancer (INCa), Fondation de France, Cancéropôle Ile-de-France, Fondation

Bettencourt-Schueller, Swiss Bridge Foundation, the LabEx Immuno-Oncology, the Institut national du cancer (SIRIC) Stratified Oncology Cell DNA Repair and Tumor Immune Elimination (SOCRATE); the SIRIC Cancer Research and Personalized Medicine (CARPEM), and the Paris Alliance of Cancer Research Institutes (PACRI). S.M. was supported by NIH (R01 CA161879, as Principal Investigator). M.C. was supported by the Fondation pour la Recherche Médicale, the Fondation ARC pour la recherche sur le cancer, and Institut Nationale du Cancer. N.W. is a recipient of a Postdoctoral Fellowship from the Agence Nationale de la Recherche. A.S. was supported by BMSI YIG 2014. F.G. is supported by SIgN core funding. L.Z., M.C., and I.B.G. are all sponsored by Association pour la Recherche contre le Cancer (PGA120140200851). F.C. was supported by INCA-DGOS (GOLD H78008). N.C. was supported by INCA-DGOS (GOLD study; 2012-1-RT-14-IGR-01). L'Oreal awarded a prize to M.V. We are grateful to the staff of the animal facility of Gustave Roussy and Institut Pasteur. We thank P. Gonin, B. Ryffel, T. Angelique, N. Chanthapathet, H. Li, and S. Zuberogoitia for technical help. DNA sequence reads from this study have been submitted to the NCBI under the Bioproject IDPRJNA299112 and are available from the Sequence Read Archive (SRP Study accession SRP065109; run accession numbers SRR2758006, SRR2758031, SRR2758178, SRR2758179, SRR2758180, SRR2758181, SRR2768454, and SRR2768457.

REFERENCES AND NOTES

1. Peggs KS, Quezada SA, Korman AJ, Allison JP. Curr Opin Immunol. 2006; 18:206–213. [PubMed: 16464564]
2. Hodi FS, et al. N Engl J Med. 2010; 363:711–723. [PubMed: 20525992]
3. Beck KE, et al. J Clin Oncol. 2006; 24:2283–2289. [PubMed: 16710025]
4. Berman D, et al. Cancer Immun. 2010; 10:11. [PubMed: 21090563]
5. Viaud S, et al. Science. 2013; 342:971–976. [PubMed: 24264990]
6. Rogoz A, Reis BS, Karssemeijer RA, Mucida D. J Immunol Methods. 2015; 421:89–95. [PubMed: 25841547]
7. Dasgupta S, Erturk-Hasdemir D, Ochoa-Reparaz J, Reinecker HC, Kasper DL. Cell Host Microbe. 2014; 15:413–423. [PubMed: 24721570]
8. Mazmanian SK, Liu CH, Tzianabos AO, Kasper DL. Cell. 2005; 122:107–118. [PubMed: 16009137]
9. Stingele F, et al. J Immunol. 2004; 172:1483–1490. [PubMed: 14734725]
10. Tzianabos AO, et al. J Biol Chem. 1992; 267:18230–18235. [PubMed: 1517250]
11. Huang JY, Lee SM, Mazmanian SK. Anaerobe. 2011; 17:137–141. [PubMed: 21664470]
12. Arumugam M, et al. Nature. 2011; 473:174–180. [PubMed: 21508958]
13. Qin J, et al. Nature. 2010; 464:59–65. [PubMed: 20203603]
14. Cebula A, et al. Nature. 2013; 497:258–262. [PubMed: 23624374]
15. Sonnenburg JL, Chen CT, Gordon JI. PLOS Biol. 2006; 4:e413. [PubMed: 17132046]
16. Lam W, et al. Sci Transl Med. 2010; 2:45ra59.
17. Xu H, et al. Nature. 2014; 513:237–241. [PubMed: 24919149]
18. Mimee M, Tucker AC, Voigt CA, Lu TK. Cell Systems. 2015; 1:62–71.

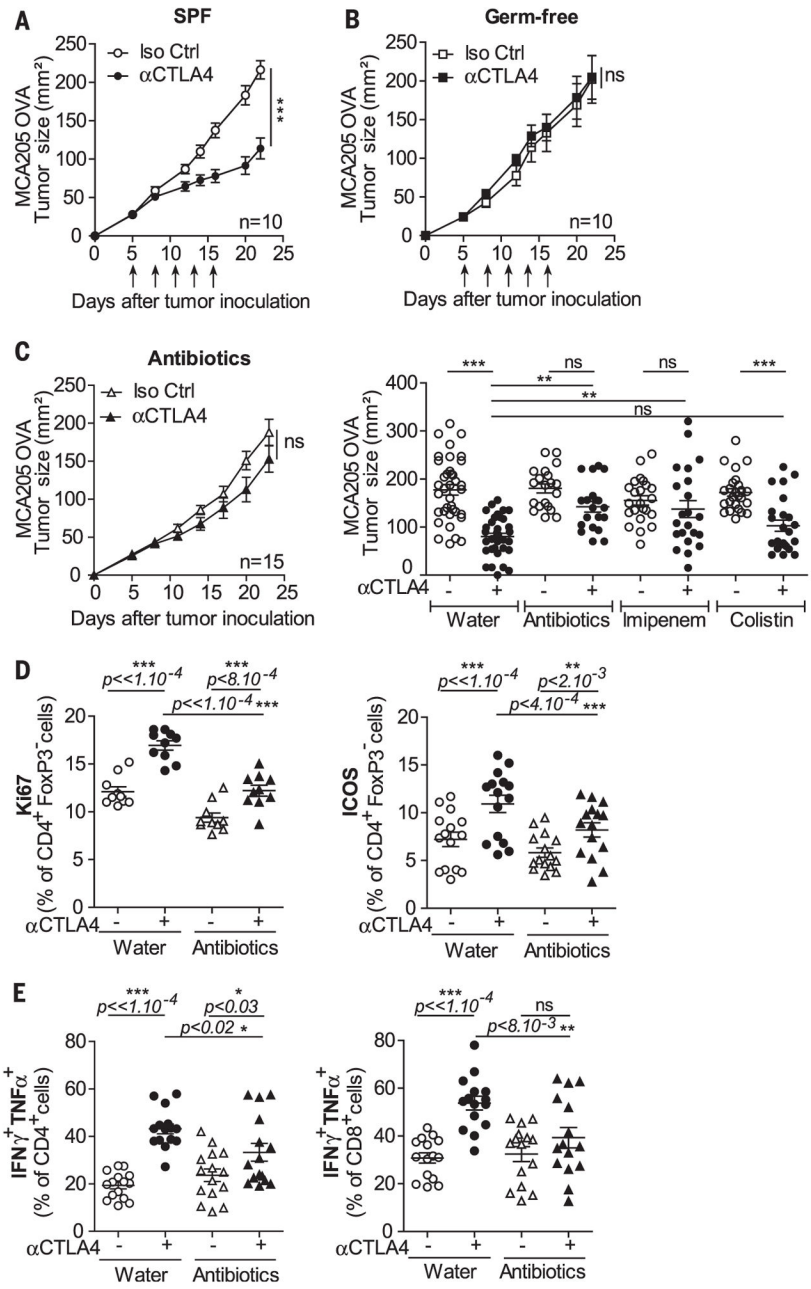

Fig. 1. Microbiota-dependent immunomodulatory effects of CTLA-4 Ab

Tumor growth of MCA205 in SPF (**A**) or GF (**B**) mice treated with five injections (compare the arrows) of 9D9 or isotype control (Iso Ctrl) Ab. (**C**) Tumor growth as in (A) and (B) in the presence (left) of ACS or (right) of single-antibiotic regimen in >20 mice per group. Flow cytometric analyses of (**D**) Ki67 and ICOS expression and (**E**) TH_1 cytokines on splenic $CD4^+Foxp3^-$Tcells (D) and TILs (E) 2 days after the third administration of 9D9 or Iso Ctrl Ab. Each dot represents one mouse in two to three independent experiments of five mice per group. *P* values corrected for interexperimental baseline variation between three individual experiments in (D). **P* < 0.05; ***P* < 0.01; ****P* < 0.001; ns, not significant.

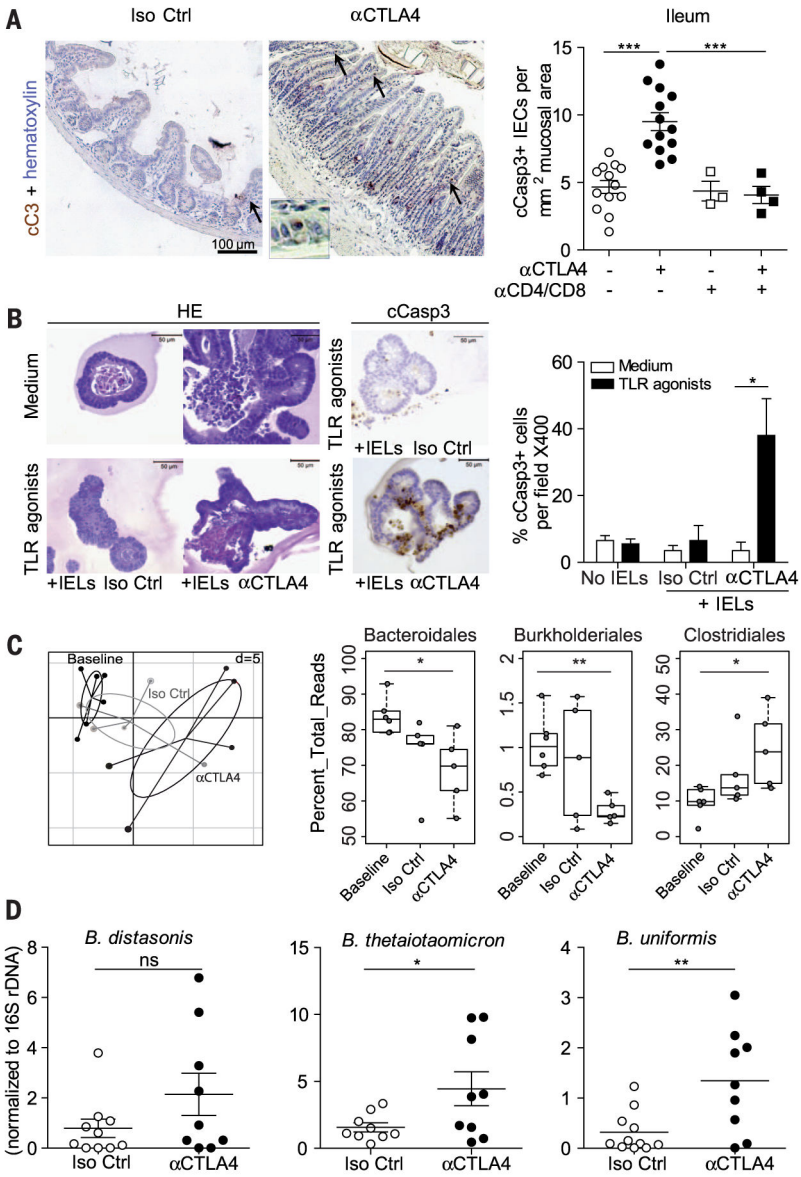

Fig. 2. IEC-IEL dialogue causes IEC apoptosis and intestinal dysbiosis after CTLA-4 Ab injection

(**A**) (left) Representative micrograph pictures of distal ileum after staining with Ab-cleaved caspase 3 (cCasp3) Ab 24 hours after one injection of 9D9 (or Iso Ctrl) Ab in naïve mice with or without prior depletion of $CD4^+$ and $CD8^+$ T cells. Inset enlarged 18-fold. (Right) Concatanated data of two experiments. (**B**) (left) Representative micrographs of 3D enteroid cocultures stimulated (or not) with TLR agonists and incubated with IELs harvested from 9D9 (or Iso Ctrl) Ab–treated mice in hematoxylin and eosin (H&E), then (middle) stained with cCasp3-specific Ab. (Right) Data concatenated from two experiments counting the means ± SEM percentages of apoptotic cells to organoid in 20 organoids. (**C**) Sequencing of 16*S* rRNA gene amplicons of feces from tumor bearers before and 48 hours after one administration of 9D9 or Iso Ctrl Ab. (Left) Principal component analysis (PCA) on a relative abundance matrix of genus repartition highlighting the clustering between baseline,

Iso Ctrl Ab–, and 9D9 Ab–treated animals after one injection (five to six mice per group). Ellipses are presented around the centroids of the resulting three clusters. The first two components explain 34.41% of total variance (Component 1: 20.04%; Component 2: 14.35%) (Monte-Carlo test with 1000 replicates, $P = 0.0049$). (C) (right) Means ± SEM of relative abundance for each three orders for five mice per group are shown. (**D**) QPCR analyses targeting three distinct *Bacteroides* spp. in ileal mucosae performed 24 to 48 hours after Ab introduction. Results are represented as $2^{-\Delta\Delta Ct} \times 10^3$, normalized to 16*S* rDNA and to the basal time point (before treatment). Each dot represents one mouse in two gathered experiments. *$P < 0.05$; ** $P < 0.01$; ***$P < 0.001$; ns, not significant.

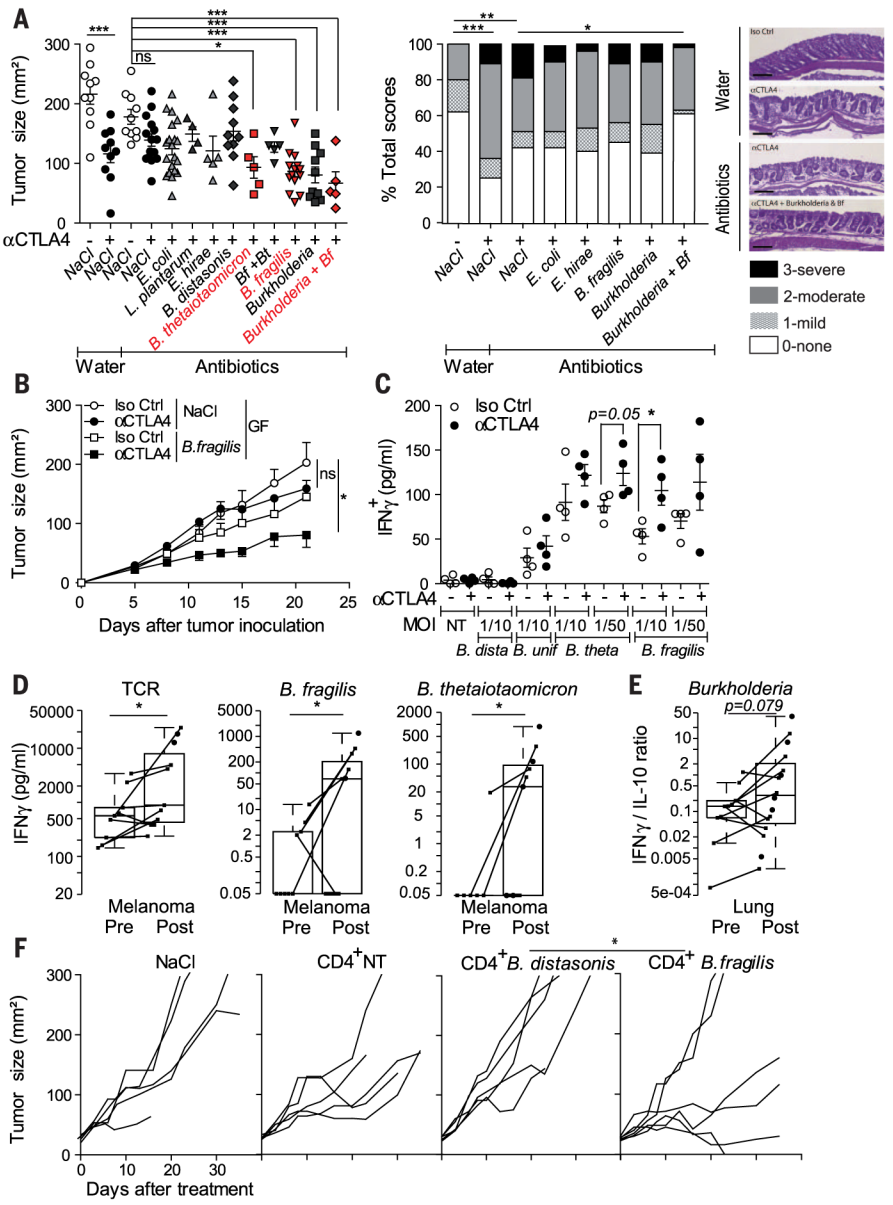

Fig. 3. Memory Tcell responses against B*t* and B*f* and anticancer efficacy of CTLA-4 blockade

(**A** and **B**) Tumoricidal effects of *Bf*, *Bt*, and/or *B. cepacia* (*Bc*) administered by oral feeding of ACS-treated or GF mice (also refer to fig. S8A). (A) (left) Tumor sizes at day 15 after 9D9 or Iso Ctrl Ab treatment are depicted. Each dot represents one tumor, and graphs depict two to three experiments of five mice per group. (Middle) Histopathological score of colonic mucosae in ACS-treated tumor bearers receiving 9D9 Ab after oral gavage with various bacterial strains, assessed on H&E-stained colons monitoring microscopic lesions as described in materials and methods at day 20 after treatment in five animals per group on at least six independent areas. (Right) Representative micrographs are shown; scale bar, 100 μm. (B) Tumor-icidal effects of *Bf* in GF mice as indicated. (**C** to **E**) Recall responses of $CD4^+$ T cells in mice and patients to various bacterial strains after CTLA-4 blockade. DCs loaded with bacteria of the indicated strain were incubated with $CD4^+$ T cells, 2 days after

three intraperitoneal (ip) CTLA-4 Ab in mice, and after at least two injections of ipilimumab (ipi) in patients. The graphs represent interferon-γ (IFN-γ) concentrations from coculture supernatants at 24 hours in mice (C) and 48 hours in MM patients (D). (E) IFN-γ/IL-10 ratios were monitored in DC–T cell cocultures of NSCLC patients at 48 hours. No cytokine release was observed in the absence of bacteria or Tcells (fig. S11 with HV). Each dot represents one patient or mouse. Paired analyses are represented by linking dots pre- and post-ipi. (**F**) Tcells harvested from spleens of mice exposed to CTLA-4 Ab and restimulated with *Bf* versus *B. distasonis* or bone marrow DCs alone ($CD4^+$ NT) were infused intravenously in day 6 MCA205 tumor-bearing GF mice. A representative experiment containing five to six mice per group is shown. **P* < 0.05; ***P* < 0.01; ****P* < 0.001; ns, not significant.

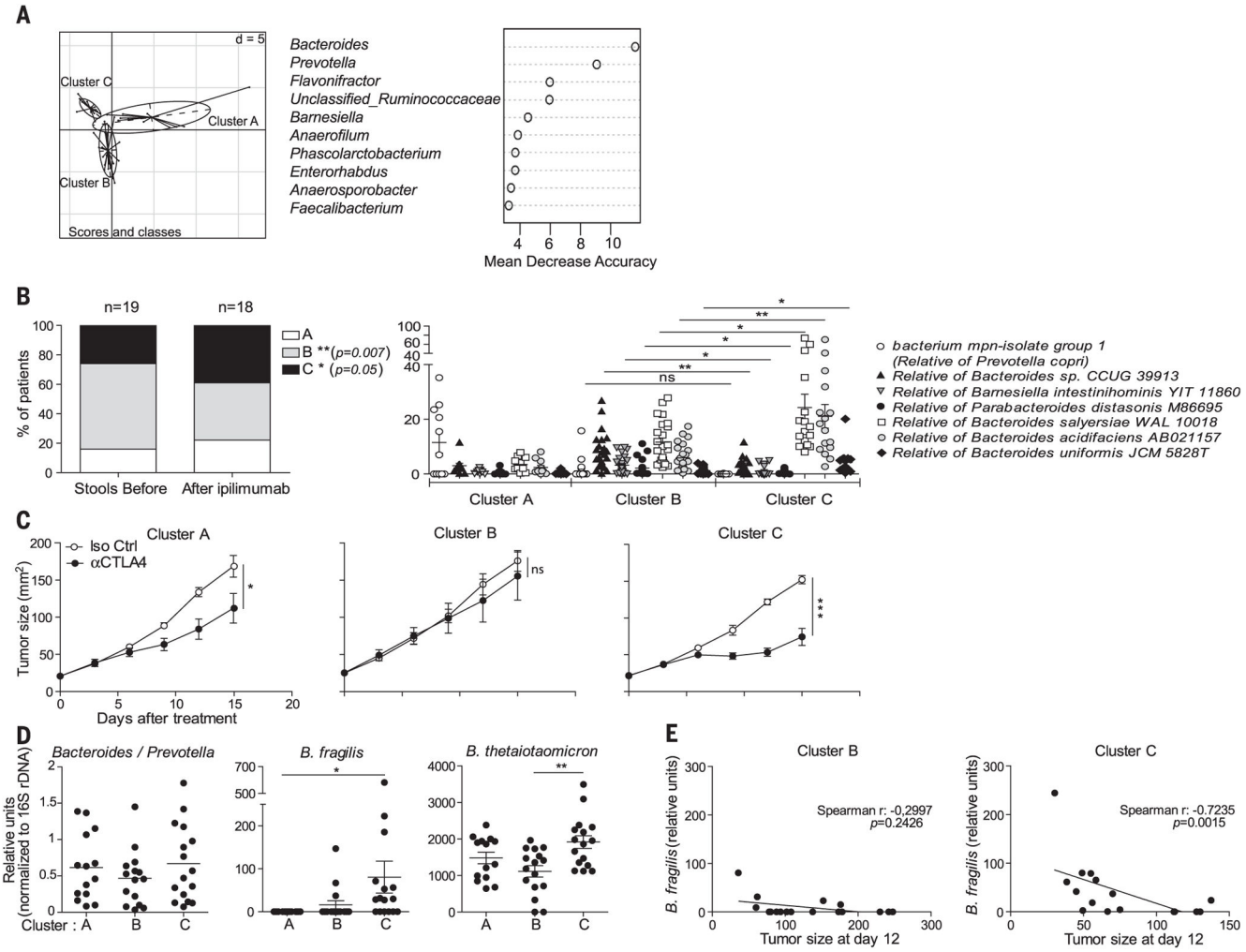

Fig. 4. Biological significance of ipilimumab-induced dysbiosis in patients

The *k* means clustering algorithm was applied on the basis of genus composition before and during ipilimumab treatment in 25 MM patients, validated using the Calinski-Harabasz index (14), and showed good performance in recovering three clusters before and after therapy (interclass PCA); (**A**) (left) (Monte-Carlo test, $P = 0.000199$). (A) (right) Random Forest analysis was applied to decipher the main genera responsible for this significant clustering. (**B**) (right) The relative abundance of main *Bacteroides* spp. significantly differed between clusters B and C. (B) (left) The proportions of patients falling into each cluster were analyzed in a nonpaired manner before versus after ipi injections regardless of the time point (fig. S20A). (**C**) Fecal microbial transplantation after introduction of ipilimumab from eight patients falling into each of the three clusters (stool selection for fecal microbial transplantation marked with an asterisk * in fig. S20A) into GF animals. One representative experiment out of three is shown with means ± SEM of tumor sizes depicted for each cluster over time. (**D**) QPCR analyses of feces DNA of the recipient before (2 weeks postcolonization) and 2 weeks after ipi, targeting *Bacteroidales* and *Bacteroides* spp. Results are represented as $2^{-\Delta Ct} \times 10^3$, normalized to 16*S* rDNA. No significant difference in the relative abundance of *Bf* was detectable in the donors of cluster B versus C before

colonization (not shown). (**E**) Spearman correlations between the amount of *Bf* in stools 15 days after treatment with 9D9 Ab and tumor sizes across cluster B- and C-recipient mice. *$P < 0.05$; **$P < 0.01$; ***$P < 0.001$.